

## **Chandra detects low-luminosity AGN with $M_{\text{BH}} = 10^4 - 10^6 M_{\odot}$ in nearby ( $z < 0.5$ ), dwarf and star-forming galaxies**

MAINAK SINGHA <sup>1,2,3</sup> JULISSA SARMIENTO,<sup>4</sup> SANGEETA MALHOTRA <sup>1</sup> JAMES E. RHOADS,<sup>1</sup> L. Y. AARON YUNG <sup>5</sup>  
JUNXIAN WANG,<sup>6</sup> ZHEN-YA ZHENG <sup>7,8</sup> RUQIU LIN,<sup>7,8</sup> KEUNHO KIM <sup>9</sup> JIALAI KANG,<sup>10</sup> AND SANTOSH HARISH<sup>11</sup>

<sup>1</sup>*Astrophysics Science Division, NASA, Goddard Space Flight Center, Greenbelt, MD 20771, USA*

<sup>2</sup>*Department of Physics, The Catholic University of America, Washington, DC 20064, USA*

<sup>3</sup>*Center for Research and Exploration in Space Science and Technology, NASA, Goddard Space Flight Center, Greenbelt, MD 20771, USA*

<sup>4</sup>*Department of Physics and Astronomy, University of Pittsburgh, Pittsburgh, PA 15260, USA*

<sup>5</sup>*Space Telescope Science Institute, 3700 San Martin Drive, Baltimore, MD 21218, USA*

<sup>6</sup>*CAS Key Laboratory for Research in Galaxies and Cosmology, Department of Astronomy, University of Science and Technology of China, Hefei 230026, China*

<sup>7</sup>*Key Laboratory for Research in Galaxies and Cosmology, Shanghai Astronomical Observatory, Chinese Academy of Sciences, 80 Nandan Road, Shanghai 200030, China*

<sup>8</sup>*School of Astronomy and Space Sciences, University of Chinese Academy of Sciences, Beijing 100049, China*

<sup>9</sup>*IPAC, California Institute of Technology, 1200 E. California Boulevard, Pasadena, CA 91125, USA*

<sup>10</sup>*University of Science and Technology of China, Hefei 230026, People's Republic of China*

<sup>11</sup>*Laboratory for Multiwavelength Astrophysics, School of Physics and Astronomy, Rochester Institute of Technology, 84 Lomb Memorial Drive, Rochester, NY 14623, USA*

### ABSTRACT

We searched the Chandra and XMM archives for observations of 900 green pea galaxies to seek signatures of AGN. Green peas are low-mass galaxies with prominent emission lines, and have remarkably similar properties (such as size, star formation rate) compared to redshift,  $z > 7$  dwarf galaxies. Out of the 29 observations found in the archives, 9 show detections in X-rays at  $S/N > 3$ . The upper limits of others are also pretty similar. The 2-10 keV X-ray luminosity for the 9 sources exceeds  $10^{40}$  erg s<sup>-1</sup>, and 2 sources show 2-10 keV X-ray luminosity greater than  $10^{41}$  erg s<sup>-1</sup>, suggesting the presence of intermediate mass black holes (IMBH)/low-luminosity AGN (LLAGN), corresponding to BH mass,  $M_{\text{BH}} = 100 - 10^6 M_{\odot}$ . All of the X-ray detected sources (plus 6 additional sources) show He II $\lambda$ 4686 emission and a broad component of the H $\alpha$  emission line indicating the presence of winds. The line widths of the broad H $\alpha$  and He II $\lambda$ 4686 emitting gas clouds are only weakly correlated ( $R^2 = 0.15$ ), suggesting that He II $\lambda$ 4686 emission is inconsistent with winds from super-Eddington accretors. However, the ratio of X-ray luminosity to star-formation rate is consistent with an anti-correlation with metallicity for 5 out of 9 sources with X-ray detection. Such anti-correlation suggests that ultraluminous X-ray sources could be the key contributors to the observed X-ray luminosity, which could be either: (i) super-Eddington accretors, or (ii) intermediate mass black holes (IMBH). The observed X-ray emission is at least an order of magnitude higher than what could be produced by Wolf-Rayet stars and fast radiative shocks from supernovae-driven winds. The X-ray luminosity in all 9 sources could, therefore, only be explained by black holes with masses exceeding  $100 M_{\odot}$ . Our results suggest that the X-ray emission in our sources requires a LLAGN. The line widths of broad H $\alpha$ , if due to accretion onto massive BH, imply masses of  $M_{\text{BH}} = 10^4 - 10^6 M_{\odot}$ . Since Green Peas have been shown to be significant Lyman Continuum leakers, the presence of LLAGN in these galaxies would imply that that such AGN might have significantly contributed to the cosmic reionization.

**Keywords:** galaxies:Galaxy, Lyman-alpha, Star-formation, AGN

### 1. INTRODUCTION

A fundamental unsolved problem in observational cosmology galaxy formation is the role of accreting supermassive black holes (SMBH) or active galactic nuclei (AGN) in ionizing the universe during the cosmic reionization. AGN fuelled by the accreting energy are more efficient in producing hard-ionizing photons—such as He II $\lambda$ 4686 (Giallongo et al.

2015; Yung et al. 2021). This leads to many studies propose the idea that AGN might have served as a significant source of ionizing photons, compared to starburst-driven processes (Madau & Haardt 2015; Volonteri et al. 2016). Whereas the general consensus is that the AGN number density is insufficiently high at elevated redshifts to accomplish complete reionization. Instead, it is widely believed that galactic ultra-

violet (UV) sources play a key role in this process (Robertson et al. 2015; Naidu et al. 2020; Yung et al. 2020a,b). Nevertheless, it is imperative that AGN can only dominate the reionization energy budget if there is an AGN abundance at  $z > 5$ .

Recent JWST observations have reported an overdensity of AGN within the redshift range  $z = 4 - 12$ . These AGN span a broad range in their Eddington ratios ( $\lambda_{\text{Edd}} = 0.06 - 2$ ), bolometric luminosities ( $L_{\text{bol}} = 10^{43} - 10^{46} \text{ erg s}^{-1}$ ), and black hole masses ( $M_{\text{BH}} = 10^5 - 10^8 M_{\odot}$ ) (Harikane et al. 2023; Larson et al. 2023; Juodžbalis et al. 2023). Studies employing JWST/NIRSpec observations propose a lower limit for unobscured AGN fractions between  $z = 6.5 - 12$ , estimated at approximately 5% (Juodžbalis et al. 2023; Xu et al. 2023). A recent JWST/MIRI imaging study reported that around 25% of galaxies in their sample at redshifts  $z = 3 - 5$  harbor heavily obscured AGN and composite AGN (Yang et al. 2023). This discovery suggests a threefold increase in the rate of black hole growth at these redshifts, exceeding expectations based on X-ray data. Such findings have substantial implications for our understanding of cosmic reionization, as accelerated black hole growth may imply an overdensity at these redshifts. Additionally, popular black hole growth models suggest that unobscured AGN is a direct result of the obscuring gas clouds being blown out by the AGN-driven superwinds (Alexander & Hickox 2012). However, we need to keep in mind that at  $z > 5$ : (1) AGN observations are relatively scarce, and (2) dwarf starburst galaxies dominate the overall galaxy population (Robertson et al. 2015; Atek et al. 2024). Therefore, local analogs of  $z > 5$  AGN host galaxies provide us with an attractive opportunity to better predict the presence of the first black holes, understand their properties and growth scenarios, and quantify their potential role in cosmic reionization.

Nearby ( $z \sim 0.3$ ), low-metallicity dwarf galaxies also known as green peas (Cardamone et al. 2009) have garnered significant attention due to their remarkable similarities with  $z > 5$  Ly $\alpha$  galaxies as seen from recent JWST spectroscopic observations (Rhoads et al. 2023). Such similarities include having subsolar metallicities, [O III] $\lambda 5007\text{\AA}$  rest-frame equivalent width exceeding  $500\text{\AA}$  half-light radius,  $r_{50} < 0.3$  kpc, and an interacting nature (Izotov et al. 2011b; Malhotra et al. 2012; Henry et al. 2015; Yang et al. 2016).

In the past two decades, X-ray observations have extensively searched for AGN in Lyman $\alpha$  emitters at redshifts  $z > 2$  (Malhotra et al. 2003; Basu-Zych & Scharf 2004; Wang et al. 2004; Yang et al. 2009; Zheng et al. 2012; Calhau et al. 2020). A commonly used indicator for AGN identification is the 2-10 keV X-ray luminosity,  $L_{2-10 \text{ keV}} > 10^{42} \text{ erg s}^{-1}$  (Nandra et al. 2002; Haines et al. 2012; Birchall et al. 2022). However, solely focusing on high-luminosity AGN might overlook those with lower luminosities ( $L_{2-10 \text{ keV}} <$

$10^{42} \text{ erg s}^{-1}$ ). For instance, our Milky Way’s supermassive black hole, Sgr A\*, has a quiet-state X-ray luminosity of  $L_{2-10 \text{ keV}} \sim 10^{33-35} \text{ erg s}^{-1}$  (Sabha et al. 2010). Recent IXPE observations have shown flaring events boosting its X-ray luminosity to  $L_{1-100 \text{ keV}} \sim 10^{39-44} \text{ erg s}^{-1}$  (Marin et al. 2023). Other studies have identified LLAGN with  $L_{2-10 \text{ keV}} \sim 10^{37-42} \text{ erg s}^{-1}$  (She et al. 2018; Diaz et al. 2020). Additionally, X-ray coronal destruction events can drastically reduce X-ray luminosity, as seen in a changing-look AGN (Ricci et al. 2020).

However, lowering the luminosity threshold may misidentify non-AGN sources such as super-Eddington accretors, which are essentially stellar mass black holes or neutron stars and are a class of high-mass X-ray binaries (HMXBs). In low-metallicity dwarf galaxies, HMXBs contribute significantly, with luminosities reaching  $10^{41} \text{ erg s}^{-1}$  (Lehmer et al. 2021, 2022). However, these HMXBs could be either super-Eddington accretors or IMBH/LLAGN, with their 2-10 keV luminosities often exceeding  $10^{39} \text{ erg s}^{-1}$  (Swartz et al. 2011; Kaaret et al. 2017), which are often termed ultraluminous X-ray sources (ULXs). Despite being long believed to host IMBHs, there has been a plethora of evidence showing ULXs may actually contain super-Eddington neutron star accretors (Sutton et al. 2013; Bachetti et al. 2014; Karino & Miller 2016; Israel et al. 2017; Pintore et al. 2018). Therefore, relying solely on X-ray observations cannot definitively determine the presence of LLAGN, necessitating additional constraints.

Optical emission lines such as H $\alpha$ , and He II $\lambda 4686$ , combined with X-ray observations could be an incredibly powerful tool to constrain the origin of X-ray emission (Fabrika et al. 2015; Lin et al. 2018). For example, Fabrika et al. (2015) found that the line-widths of He II $\lambda 4686$  and H $\alpha$  shows almost a one-to-one correlation for super-Eddington accretors, where such high accretion rate almost always launches a very strong wind (Shakura & Sunyaev 1973). In this paper, we adopt this approach to investigate whether green peas truly host low luminosity AGN.

This paper is organized as follows: In Section 2, we first briefly describe the data. We then investigate the multi-wavelength data and outline the main results in Section 3, while in Section 4 we combine the results from the observations and attempt to explain the origin of any observed multi-wavelength emission mechanisms and their potential connection to AGN. Finally in Section 5 we present our conclusions.

## 2. OBSERVATION AND DATA

### 2.1. Sample Selection:

We began with the parent sample of green pea galaxies from Jiang et al. (2019). This consists of 1004 objects selected from Data Release 13 of the Sloan Digital Sky Survey (SDSS DR13). The primary selection was for high equiva-

**Table 1.** Host galaxy properties of green peas

Object	RA	DEC	Redshift	SFR ( $M_{\odot} \text{ yr}^{-1}$ )	12+log(O/H)	X-ray detection	He II detection
J173501.2+570308	263.76	57.05	0.091	14.04	8.26	True	True
J002101.0+005248	5.25	0.88	0.077	8.00	8.22	True	True
J084414.2+022620	131.06	2.44	0.066	5.06	8.10	True	True
J093813.5+542824	144.56	54.47	0.047	10.19	8.07	True	True
J080619.5+194927	121.58	19.82	0.102	13.56	8.27	True	True
J141059.2+430247	212.75	43.05	0.07	9.84	8.29	True	True
J140956.6+545648	212.49	54.95	0.098	13.71	8.23	True	True
J162410.10-002202.5	246.04	-0.37	0.031	3.98	8.24	True	True
SHOC 486	22.02	-1.18	0.027	2.77	8.07	True	True
J121903.98+152608.5	184.77	15.44	0.196	12.96	7.87	False	True
J101629.88+073404.9	154.12	7.57	0.183	16.94	8.18	False	False
J164235.52+422349.7	250.65	42.40	0.151	16.48	8.24	False	False
J104645.75+302330.9	161.69	30.39	0.127	8.58	8.32	False	False
J121932.22+213324.9	184.88	21.56	0.141	19.06	8.21	False	True
J014721.7-091646	26.84	-9.28	0.136	4.99	8.19	False	False
J144231.37-020952.0	220.63	-2.16	0.294	21.23	8.00	False	False
J150934.17+373146.1	227.39	37.53	0.033	1.77	7.85	False	True
J160627.53+135547.8	241.61	13.93	0.107	9.28	8.20	False	True
J101526.38+305451.9	153.86	30.91	0.092	6.09	8.26	False	False
J031023.94-083432.8	47.6	-8.58	0.052	0.96	8.26	False	False
J092532.36+140313.1	141.38	14.05	0.301	23.8	8.06	False	False
J235604.67-85423.4	359.02	-8.91	0.169	9.06	8.26	False	False
J094244.23+411019.3	145.68	41.17	0.046	2.56	7.94	False	False
J132916.55+170020.9	202.32	17.01	0.094	9.95	8.22	False	True
J155027.78+192058.7	237.62	19.35	0.212	20.76	8.27	False	False
J154748.99+22303.2	236.95	22.05	0.031	0.68	8.05	False	False
J140018.93+010453.8	210.08	1.08	0.121	11.78	8.08	False	False
J154543.55+085801.3	236.43	8.97	0.038	4.43	7.76	False	True

lent width emission lines, with either the equivalent width of [O III]  $5007\text{\AA}$ ,  $EW_{5007} > 300\text{\AA}$ , or the equivalent width of the Balmer  $H\beta$  line  $EW_{H\beta} > 100\text{\AA}$ . Further details of the selection are given in Jiang et al. (2019). We cross matched this list with the *Chandra Observations Catalog* and the *Chandra Source Catalog, Version 2.0* to identify green pea galaxies where we can study X-ray emission properties. We identified 29 green peas with *CXO* observations, including 7 that are detected in the *Chandra Source Catalog*, 2 additional sources were detected with X-ray emission over  $> 3\sigma$  confidence among the remaining 22 sources.

### 2.2. Optical Data:

We used *Sloan Digital Sky Survey* optical spectra to measure the flux and flux error of the He II  $\lambda 4686$  line for the 29 sources in our sample. We considered He II  $\lambda 4686$  as detected only when the signal-to-noise ratio,  $S/N_{\text{He II}} > 3$ . Among the 9 X-ray-detected sources, 8 exhibited He II  $\lambda 4686$

detection over  $3\sigma$  confidence. Similarly, among the 20 X-ray non-detected sources, 9 displayed He II  $\lambda 4686$  detections. One source hovered at a borderline  $S/N_{\text{He II}} \sim 2.99$ . However, adopting a conservative stance, we opted to disregard this particular source due to its  $S/N < 3$ . Other emission lines used in our analysis (e.g.,  $H\alpha$  and [N II]; see section 3.2.2) are similarly measured from the *SDSS* spectra.

### 2.3. X-ray Data:

For X-ray measurements, we used measurements from the *Chandra Source Catalog, Version 2.0* for the seven sample objects contained in that catalog. We downloaded the data for the remaining 22 sources from the *Chandra X-ray Center (CXC)*, and then reduced and analyzed using the *Chandra Interactive Analysis of Observations (CIAO; v4.16)* tools (Fruscione et al. 2006). Firstly, we utilized the CIAO task *repro* to reprocess the level-1 ACIS event file data. Then we used the task *srcflux* to estimate the source counts and fluxes in the

broad band, 0.5 – 7 keV and in the hard band, 2-7 keV. For each source, we defined a circular source region centered at the source position on the broad band images, with a radius  $R_{\text{source}}$  enclosing 90% of the PSF at 1.0 keV. Backgrounds are extracted from an annulus with  $R_{\text{source}} < R < 5R_{\text{source}}$ , after confirming the absence of nearby bright X-ray sources. Out of the 22 observations, J162410.10-002202.5 and SHOC 486 are detected with significant X-ray emission (over  $3\sigma$  confidence) in both broad and hard bands. Therefore, for the sources with no X-ray detection, extracting background from a region between  $R_{\text{source}} - 5R_{\text{source}}$  should not introduce any uncertainty. For 162410.10-002202.5 and SHOC 486, the background may be slightly overestimated due. However, even with the overestimated background, a source detection over  $3\sigma$  strongly suggests that the detection is indeed robust.

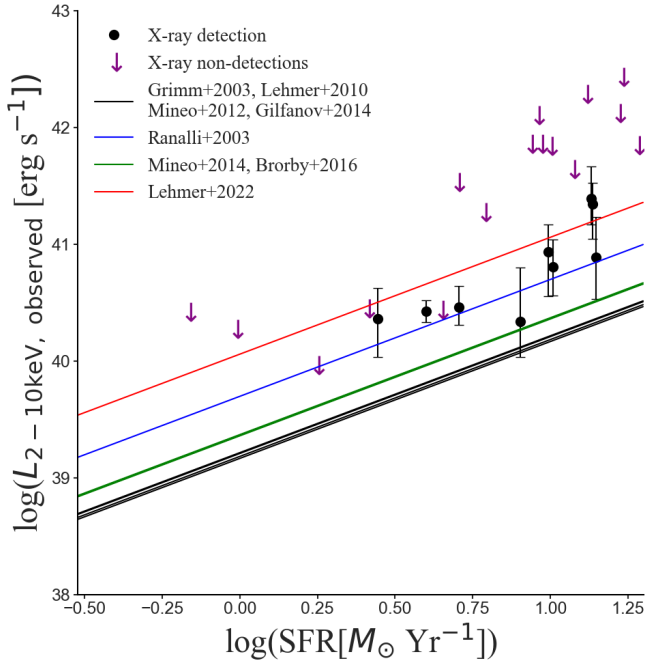


**Figure 1.** 2-10 keV observed X-ray luminosity for our sources ( $L_{2-10 \text{ keV, observed}}$ ) vs. star formation rate (SFR, derived from narrow  $H\alpha$  flux). Curves show the expected relation of  $L_{2-10 \text{ keV}}$  and SFR from the literature for several classes of galaxy. X-ray detections are shown with  $1\sigma$  uncertainties, and nondetections are plotted as XX% confidence upper limits. If our sources are similar to LIRGs, then the observed X-ray emission cannot be described by XRBs alone. However, using the low metallicity galaxy calibration,  $L_{2-10 \text{ keV, observed}}$  almost agrees with  $L_{2-10 \text{ keV, observed}}$ .

The low net counts restrict us from performing any efficient spectrum analysis. This makes the number of sources with X-ray detection over  $3\sigma$  confidence to be 9. The host galaxy properties of these sources are listed in Table 1. We present the X-ray flux values in the 0.5-7 keV, 2-7 keV bands for the sources with X-ray detections and  $3\sigma$  upper limits for

the non-detections in Table 2. We have listed the 2-10 keV X-ray luminosity values (or the upper limits) for these sources as well.

### 3. ANALYSIS AND RESULTS

#### 3.1. X-ray emission:

We employ the Chandra-based Portable, Interactive Multi-Mission Simulator (PIMMS) to convert the 0.2-5 keV X-ray fluxes to 2-10 keV unabsorbed fluxes by applying a correction factor of approximately 1.944. This correction is based on a photon index of  $\Gamma = 1.47$ , a typical value for starburst galaxies (Rephaeli et al. 1995), and a galactic hydrogen column density  $N_{\text{H}} = 3 \times 10^{20} \text{ cm}^{-2}$ . The estimated 2-10 keV X-ray luminosity for these sources spans a range of  $L_{2-10 \text{ keV, observed}} = 7.8 \times 10^{40} - 1.07 \times 10^{41} \text{ erg s}^{-1}$ . These  $L_{2-10 \text{ keV}}$  values are at least an order of magnitude higher than those typically observed in dwarf galaxies hosting AGN (Reines et al. 2014; Mezcua et al. 2018; Latimer et al. 2021), where  $L_{2-10 \text{ keV, observed}} < 10^{40} \text{ erg s}^{-1}$ . However, the SFR values in our sources are also an order of magnitude higher than their sources. In starburst galaxies, it is well-established that the X-ray binary population contribute to the observed X-ray emission significantly and that it increases with the galactic SFR. Therefore, it is necessary to estimate the 2-10 keV luminosity attributable to X-ray binaries  $L_{2-10 \text{ keV, XRB}}$ .

Despite both low mass (LMXBs) and high mass X-ray binaries (HMXBs) contributing to 2-10 keV X-ray emission, the LMXB contribution is negligible compared to the HMXBs as documented by several studies (Grimm et al. 2003; Mineo et al. 2014; Svoboda et al. 2019; Lehmer et al. 2022). We conduct a comparative analysis of the 2-10 keV X-ray luminosity of our sources with the X-ray binary (XRB) contribution, employing various  $L_{2-10 \text{ keV}}\text{-SFR-Z}$  calibrations sourced from the existing literature.

Ranalli et al. (2003) established a correlation between the star formation rates (SFRs) of a selected group of nearby star-forming galaxies and their total X-ray luminosity in the 2-10 keV range, denoted as  $L_{2-10 \text{ keV, observed}} \sim 5 \times 10^{39} \text{ SFR} (M_{\odot} \text{ Yr}^{-1})$ . It is crucial to acknowledge that in this context, SFR values are derived only from stars with masses exceeding  $5M_{\odot}$ . A study by Grimm et al. (2003) suggested an XRB luminosity scaling with the SFR, expressed as  $L_{2-10 \text{ keV, observed}} \sim 1.65 \times 10^{39} \text{ SFR} (M_{\odot} \text{ Yr}^{-1})$  in the 2-10 keV band. Lehmer et al. (2010) prescribed a calibration very similar to Grimm et al. (2003),  $L_{2-10 \text{ keV, observed}} \sim 1.62 \times 10^{39} \text{ SFR} (M_{\odot} \text{ Yr}^{-1})$  for luminous infrared galaxies (LIRGs). In the mid-infrared color-color diagram, the sources in our sample occupy similar regions as the luminous infrared galaxies (LIRGs) or ultra-luminous infrared galaxies (ULIRGs) as shown by Harish et al. (2021).

**Table 2.** X-ray properties of green peas

Object	$F_{2-7 \text{ keV}}$ [ $10^{-15} \text{ erg s}^{-1} \text{ cm}^{-2}$ ]	$F_{0.5-7 \text{ keV}}$ [ $10^{-15} \text{ erg s}^{-1} \text{ cm}^{-2}$ ]	$\log(L_{2-10 \text{ keV}})$ [ $\text{erg s}^{-1}$ ]	$\log\beta=\log(L_{0.5-8 \text{ keV}}/\text{SFR})$ [ $\text{erg s}^{-1} (M_{\odot} \text{ yr}^{-1})^{-1}$ ]
J173501.2+570308	$2.61^{+2.06}_{-2.07}$	$4.31^{+1.79}_{-1.79}$	$40.89^{+0.36}_{-0.35}$	$39.86^{+0.25}_{-0.19}$
J002101.0+005248	$1.04^{+0.86}_{-0.86}$	$2.8^{+1.05}_{-1.05}$	$40.34^{+0.3}_{-0.46}$	$39.76^{+0.15}_{-0.19}$
J084414.2+022620	$1.96^{+0.77}_{-0.77}$	$2.98^{+1.18}_{-1.18}$	$40.46^{+0.16}_{-0.18}$	$39.84^{+0.2}_{-0.17}$
J093813.5+542824	$8.52^{+3.93}_{-3.93}$	$13.5^{+3.49}_{-3.7}$	$40.81^{+0.25}_{-0.24}$	$39.89^{+0.15}_{-0.11}$
J080619.5+194927	$6.53^{+2.8}_{-2.96}$	$9.72^{+2.64}_{-2.64}$	$41.39^{+0.23}_{-0.27}$	$40.33^{+0.12}_{-0.15}$
J141059.2+430247	$5.05^{+2.46}_{-2.46}$	$9.75^{+2.05}_{-2.04}$	$40.93^{+0.38}_{-0.24}$	$40.12^{+0.09}_{-0.09}$
J140956.6+545648	$6.35^{+3.54}_{-2.54}$	$11.7^{+2.27}_{-2.43}$	$41.35^{+0.3}_{-0.18}$	$40.37^{+0.09}_{-0.1}$
J162410.10-002202.5	$8.32^{+1.9}_{-1.8}$	$20.2^{+1.9}_{-2.2}$	$40.43^{+0.1}_{-0.09}$	$40.11^{+0.04}_{-0.05}$
SHOC 486	$9.4^{+5.91}_{-4.6}$	$14.3^{+9.1}_{-7.0}$	$40.36^{+0.33}_{-0.26}$	$40.0^{+0.22}_{-0.26}$
J121903.98+152608.5	< 12.42	< 18.93	< 42.29	< 41.25
J101629.88+073404.9	< 20.04	< 30.54	< 42.43	< 41.28
J164235.52+422349.7	< 14.96	< 22.8	< 42.12	< 40.98
J104645.75+302330.9	< 11.95	< 18.21	< 41.86	< 41.0
J121932.22+213324.9	< 9.24	< 14.08	< 41.85	< 40.64
J014721.7-091646	< 4.86	< 7.4	< 41.53	< 40.91
J144231.37-020952.0	< 11.95	< 18.21	< 42.67	< 41.42
J150934.17+373146.1	< 2.63	< 4.0	< 39.96	< 39.79
J160627.53+135547.8	< 17.13	< 26.1	< 41.86	< 40.97
J101526.38+305451.9	< 6.22	< 9.48	< 41.27	< 40.57
J031023.94-083432.8	< 2.08	< 3.17	< 40.27	< 40.37
J092532.36+140313.1	< 6.13	< 9.34	< 42.41	< 41.11
J235604.67-85423.4	< 11.29	< 17.21	< 42.1	< 41.22
J094244.23+411019.3	< 3.97	< 6.05	< 40.45	< 40.12
J132916.55+170020.9	< 21.83	< 33.27	< 41.84	< 40.92
J155027.78+192058.7	< 13.74	< 20.94	< 42.41	< 41.17
J154748.99+22303.2	< 8.14	< 12.4	< 40.42	< 40.67
J140018.93+010453.8	< 8.05	< 12.27	< 41.64	< 40.65
J154543.55+085801.3	< 5.82	< 8.88	< 40.44	< 39.87

Mineo et al. (2012) considered the contribution from stars within the mass range of  $0.1\text{-}1000M_{\odot}$ , resulting in  $L_{2-10 \text{ keV, XRB}} \sim 1.53 \times 10^{39} \text{ SFR} (M_{\odot} \text{ Yr}^{-1})$ . Notably, their study focused solely on resolved star-forming galaxies. Gilfanov & Merloni (2014) observed a closely analogous correlation, with  $L_{2-10 \text{ keV, XRB}} \sim 1.47 \times 10^{39} \text{ SFR} (M_{\odot} \text{ Yr}^{-1})$ . Conversely, Mineo et al. (2014) studied the X-ray properties of compact (unresolved) star-forming galaxies, yielding significantly higher X-ray luminosity values compared to Mineo et al. (2012):  $L_{2-10 \text{ keV, XRB}} \sim 2.35 \times 10^{39} \text{ SFR} (M_{\odot} \text{ Yr}^{-1})$ . It is pertinent to note that the green peas within our sample, being unresolved by Chandra, warrant a comparison of their X-ray emission not only with resolved sources but also with unresolved ones. The effect of metallicity introduces additional complexity in understanding the X-ray emission in

starburst galaxies. Brorby et al. (2016); Lehmer et al. (2019, 2022) suggested that in low-metallicity galaxies, the X-ray luminosity from HMXBs increase by  $\sim$  an order of magnitude than normal galaxies. Brorby et al. (2016) suggested a calibration among  $L_{2-10 \text{ keV}}$ , SFR and metallicity  $Z$ . Using the median metallicity for our sources  $Z \sim 0.3Z_{\odot}$ , the Brorby et al. (2016) relation translates to  $L_{2-10 \text{ keV, XRB}} \sim 2.29 \times 10^{39} \text{ SFR} (M_{\odot} \text{ Yr}^{-1})$ , which is very similar to what Mineo et al. (2014) derived. In each of these calibrations, the X-ray luminosity calibrations from XRBs fail to produce the total observed X-ray luminosity in all of our sources as seen in Fig. 1. Lehmer et al. (2022) has suggested that in low-metallicity ( $7 < 12 + \log(\text{O}/\text{H}) < 9.2$ ) dwarf galaxies, the population of ultraluminous X-ray sources or ULX ( $L_{2-10 \text{ keV}} > 2 \times 10^{39} \text{ erg s}^{-1}$ )- a subset of HMXB rises significantly and they dominantly contribute to the observed

**Table 3.** Emission line galaxy properties of green peas

Object	$\sigma_{\text{H}\alpha, \text{ broad}}$ [km s <sup>-1</sup> ]	$\sigma_{\text{He II}\lambda 4686}$ [km s <sup>-1</sup> ]	$L_{\text{H}\alpha, \text{ broad}}$ [erg s <sup>-1</sup> ]	$L_{\text{He II}\lambda 4686}$ [erg s <sup>-1</sup> ]	$S/N(\text{He II}\lambda 4686)$
J173501.2+570308	102±19	448±186	42.07±0.27	39.74±0.3	3.35
J002101.0+005248	170±15	502±112	41.44±0.2	39.97±0.22	4.49
J084414.2+022620	131±26	126±40	41.42±0.45	39.25±0.27	3.69
J093813.5+542824	181±34	162±23	41.24±0.22	39.43±0.09	10.7
J080619.5+194927	173±11	363±123	41.75±0.18	40.0±0.23	4.28
J141059.2+430247	114±20	560±115	41.74±0.5	39.9±0.21	4.79
J140956.6+545648	210±45	279±47	42.03±0.24	40.05±0.12	8.59
J162410.10-002202.5	90±30	525±139	40.32±3.0	39.46±0.2	5.01
SHOC 486	82±44	124±21	41.49±0.48	39.12±0.09	11.4
J121903.98+152608.5	227±60	104±29	41.9±0.22	40.19±0.21	4.76
J121932.22+213324.9	193±12	252±70	41.89±0.17	39.96±0.28	3.55
J150934.17+373146.1	56±36	102±45	41.1±47.66	39.02±0.11	8.71
J160627.53+135547.8	189±12	245±85	41.73±0.16	39.76±0.25	4.06
J132916.55+170020.9	198±42	821±241	41.81±0.22	40.21±0.26	3.88
J154543.55+085801.3	57±15	85±9	41.54±46.1	39.48±0.05	18.92

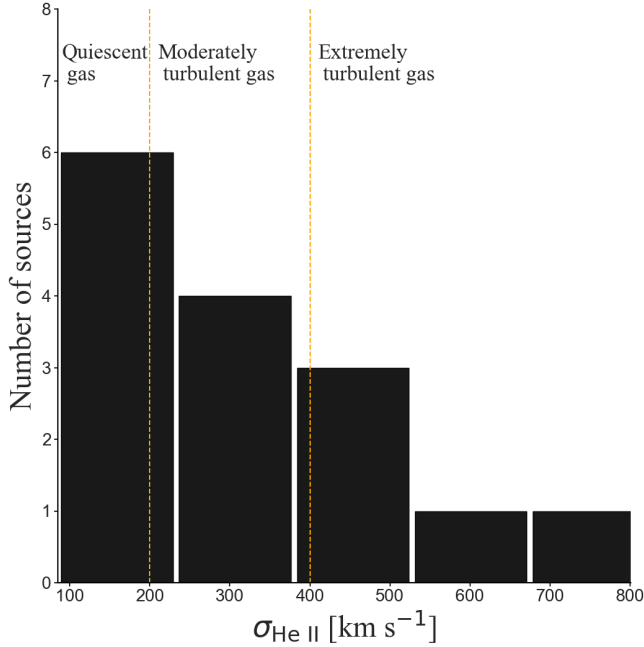


**Figure 2.** A histogram of the velocity dispersion ( $\sigma_{\text{He II}\lambda 4686}$ ) of the 15 sources where the  $S/N$  of the He II  $\lambda 4685$  emission line is  $> 3$ ,  $\sigma_{\text{He II}\lambda 4686}$ . The yellow vertical dashed lines are at  $\sigma_{\text{He II}\lambda 4686} = 200 \text{ km s}^{-1}$  and  $400 \text{ km s}^{-1}$ , and represent boundaries between sources where the He II  $\lambda 4686$  gas kinematics is quiescent ( $\sigma_{\text{He II}\lambda 4686} < 200 \text{ km s}^{-1}$ ), moderately turbulent ( $\sigma_{\text{He II}\lambda 4686} = 200 - 400 \text{ km s}^{-1}$ ), and highly turbulent gas ( $\sigma_{\text{He II}\lambda 4686} > 400 \text{ km s}^{-1}$ ).

X-ray emission. The authors noted that these ULXs may contain intermediate mass black holes, black hole or neutron star binaries.

Adopting the calibration for  $12 + \log(\text{O}/\text{H}) = 8.2$ , which corresponds to the average metallicity for our sources, we do notice that 2-10 keV X-ray luminosity can be described by the calibration of [Lehmer et al. \(2022\)](#). However, in J0801619.5+194927 and J140956.6+54568,  $L_{2-10 \text{ keV}}$  exceeds  $10^{41} \text{ erg s}^{-1}$ . Sources with  $L_{2-10 \text{ keV}} > 10^{41} \text{ erg s}^{-1}$  are often believed to host intermediate mass black holes (IMBH,  $M_{\text{BH}} > 100 M_{\odot}$ ) ([Barrows et al. 2019](#)). Therefore, these two out of 9 sources are strong candidates to host IMBH.

### 3.2. Optical emission lines:

#### 3.2.1. He II $\lambda 4686$ emission:

For the 15 sources where  $S/N_{\text{He II}} > 3$ , we fitted the emission line spectra from 4640-4740 Å, encompassing the Fe III  $\lambda 4658$ , He II  $\lambda 4686$ , and Ar IV  $\lambda 4711$  emission lines. Modelling multiple emission lines together yielded a more robust fit. We coupled the emission line centers of the emission lines and the line-widths for Fe III  $\lambda 4658$  and Ar IV  $\lambda 4711$ . We noticed that the He II  $\lambda 4686$  lines are broader than Fe III  $\lambda 4658$  and Ar IV  $\lambda 4711$ . Attempting to couple the line-widths and line-centers of Fe III  $\lambda 4658$ , He II  $\lambda 4686$ , and Ar IV  $\lambda 4711$ , and adding a second broad Gaussian to He II  $\lambda 4686$ , did not converge the fit. The fit only converged when we did not couple the line-width of He II  $\lambda 4686$  to the other two lines.

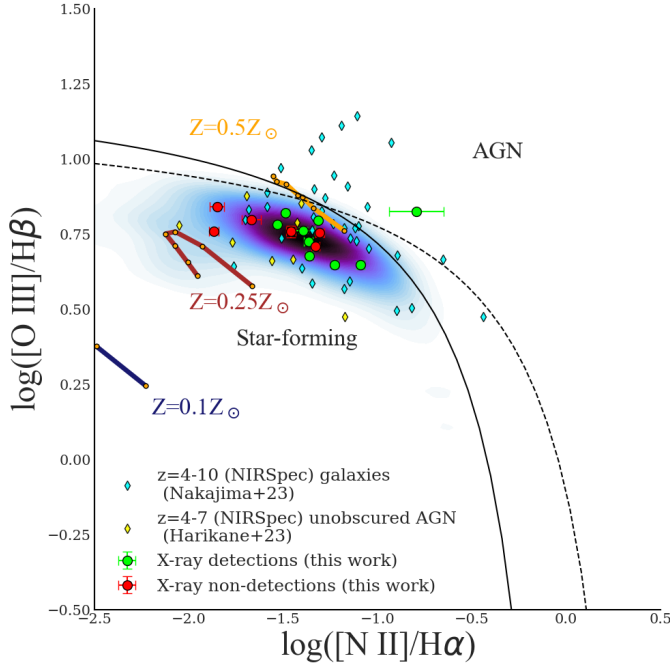


**Figure 3.** BPT diagram showing the emission line ratios of  $[\text{O III}]/\text{H}\beta$  plotted against those of  $[\text{N II}]/\text{H}\alpha$  for the parent sample of green peas (Yang et al. 2016), along with the 15 green peas with  $> 3\sigma$  He II detection. The green circles denote the sources where X-ray emission has been detected over  $> 3\sigma$  confidence and the red circles represent the ones where X-ray emission has not been detected. The black solid and dashed lines represent the boundary between star-forming galaxies and AGN as per Kewley et al. (2001); Kauffmann et al. (2003). Low metallicity AGN narrow-line regions are depicted according to Groves et al. (2006), with different solid lines representing models for AGN host galaxies with metallicities of  $Z = 0.5Z_{\odot}$  (orange line),  $0.25Z_{\odot}$  (brown line), and  $0.1Z_{\odot}$  (blue line). The orange data points on these lines represent models with different intensity and ionization parameters (see Table 2 of Groves et al. (2006)). Most of our sources lie between the models for  $Z = 0.25Z_{\odot}$  and  $Z = 0.5Z_{\odot}$ .

We report that the He II  $\lambda 4686$  emission line exhibits a great diversity in their line-width, with 1/3 of the total sample shows highly perturbed gas with  $\sigma_{\text{He II}} > 400 \text{ km s}^{-1}$ . On the contrast, narrow, nebular He II  $\lambda 4686$  emission is clearly visible with  $\sigma_{\text{He II}} < 200 \text{ km s}^{-1}$  as seen in Fig. 2.

### 3.2.2. $\text{H}\alpha$ emission

To understand the astrophysical origin of the X-ray emission, it is necessary to verify if the  $\text{H}\alpha$  and He II  $\lambda 4686$  shows a one-to-one relation, as that would directly show a presence of an super-Eddington accretor. We fit the 6530-6600Å rest-frame wavelength covering  $\text{H}\alpha + [\text{N II}]\lambda\lambda 6548, 6584$  with a multi-Gaussian model where the narrow Gaussian describes the nuclear star-cluster emission and the broad Gaussian may be due to supernovae-driven winds. The line-centers and line-widths for all  $\text{H}\alpha$  and  $[\text{N II}]$  lines

were coupled to each other for both the narrow and broad Gaussian complexes. Additionally, we constrained the  $[\text{N II}]\lambda 6584/[\text{N II}]\lambda 6548 = 2.61$  (Singha et al. 2021, 2023; Winkel et al. 2023). All of our sample shows the broad  $\text{H}\alpha$  line to be moderately turbulent at most with  $\sigma_{\text{H}\alpha} < 300 \text{ km s}^{-1}$ . These values are in agreement with the work of Wood et al. (2015), where the authors found that,  $\sigma_{\text{H}\alpha} = 70 - 300 \text{ km s}^{-1}$  due to such winds. However, other possibilities such as the gravitational potential of a massive black hole or additional star cluster (in J173501.2+570308 and SHOC 486) cannot be excluded either. The values of the velocity dispersion and the luminosity of the broad components in  $\text{H}\alpha$  and He II  $\lambda 4686$  are listed in Table. 3. All the optical spectra are presented in the Appendix.

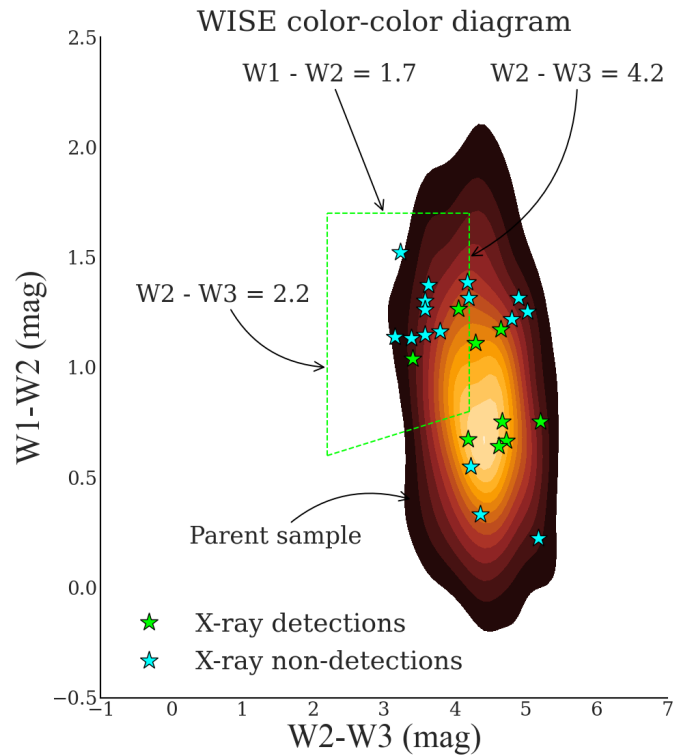


**Figure 4.** The WISE survey mid-infrared color-color plane used to identify candidate AGN among the GPs. The red contours describe the parent sample. The WISE color plane acts as a classification tools for different types of astrophysical objects, including stars, AGN and LIRGs etc. (Wright et al. 2010). The dashed box is the AGN selection region as per Jarrett et al. (2011).

### 3.2.3. Ionization mechanism

A popular diagnostic to understand the origin of the astrophysical processes responsible for multi-wavelength emission is the optical emission line diagnostics (Baldwin et al. 1981), using  $[\text{O III}]/\text{H}\beta$  and  $[\text{N II}]/\text{H}\alpha$  emission line ratios. To estimate the line ratio  $[\text{O III}]/\text{H}\beta$ , we fit the 4840-5020Å rest-frame wavelength range covering  $\text{H}\beta$  and

[O III] $\lambda\lambda$ 4959, 5007 with a single-Gaussian model and a linear model for the continuum (Singha et al. 2021, 2022), which was sufficient to describe the emission line features.

In these sources [O III]/ $H\beta$  and [N II]/ $H\alpha$ , emission line ratios are similar to those of redshift  $z > 4$  AGN detected by JWST/NIRSpec (Nakajima et al. 2023; Harikane et al. 2023), despite falling in the star-forming region of the BPT diagram (see Fig. 3). Only SHOC 486, a source with X-ray detection, falls in the AGN-photoionization regime. Groves et al. (2006) proposed that in low-metallicity AGN, the emission line ratios could mimic those of pure star-forming galaxies. In Fig. 3, we notice that 14 out of 15 sources with  $S/N(\text{He II}) > 3$  reside within the region described by the narrow-line region models for metallicity values of  $0.25Z_{\odot}$  and  $0.5Z_{\odot}$ . Given that the median metallicity for these sources is  $\sim 0.32Z_{\odot}$ , their emission line ratios are consistent with the narrow-line region of low-metallicity AGN.

### 3.3. Mid-infrared color:

The Mid-infrared (MIR) color criteria (Jarrett et al. 2011) using WISE observations ( $W_1$  at  $3.4\mu\text{m}$ ,  $W_2$  at  $4.6\mu\text{m}$ , and  $W_3$  at  $12\mu\text{m}$ ) shows that the MIR colors of our sources are similar to that of ULIRGs, LIRGs and QSOs. Out of 29 sources, the MIR color is available for 25 sources including all 9 sources with  $> 3\sigma$  X-ray detection and 16 sources with X-ray non-detection. Two out of nine sources with X-ray detection fall in the AGN regime as per the MIR color criteria suggested by Jarrett et al. (2011), shown in Fig. 4. Whereas for the sources with X-ray non-detection, ten out of sixteen sources lie in the AGN regime of the MIR color diagram. Jarrett et al. (2011) suggested that a source would be consistent with AGN only if their MIR colors satisfy  $2.2 < W_2 - W_3 < 4.2$ , and  $0.1 \times (W_2 - W_3) + 0.38 < W_1 - W_2 < 1.7$ .

In MIR wavelengths, very young compact starburst galaxies with stellar population  $<$  a few Myr can result in MIR color (Izotov et al. 2011a; Satyapal et al. 2018). However, processes driven solely by starburst activity can replicate the MIR WISE color of luminous AGNs if the ionization parameter  $\log U > -0.5$  (Abel & Satyapal 2008; Satyapal et al. 2021). Based on the optical SDSS spectra, we estimate that  $-3.1 < \log U < -2.5$  for our sample, with an average  $\text{Log } U_{\text{avg}}$  of  $-2.8 \pm 0.3$ , at a 300 pc radius (assuming an electron density of  $200 \text{ cm}^{-3}$ ), which is typically the half-light radius for these sources (Kim et al. 2021). At such moderate  $\text{Log } U$  values, only radiation from AGN accretion disk can produce these MIR colors. However, it is unclear if the MIR colors of IMBH are similar to AGN or not. Therefore, it is entirely possible that the MIR colors are produced by Compton-thick massive black holes ( $M_{\text{BH}} > 100M_{\odot}$ ), whereas they almost contribute negligibly to the X-ray emission.

## 4. DISCUSSION

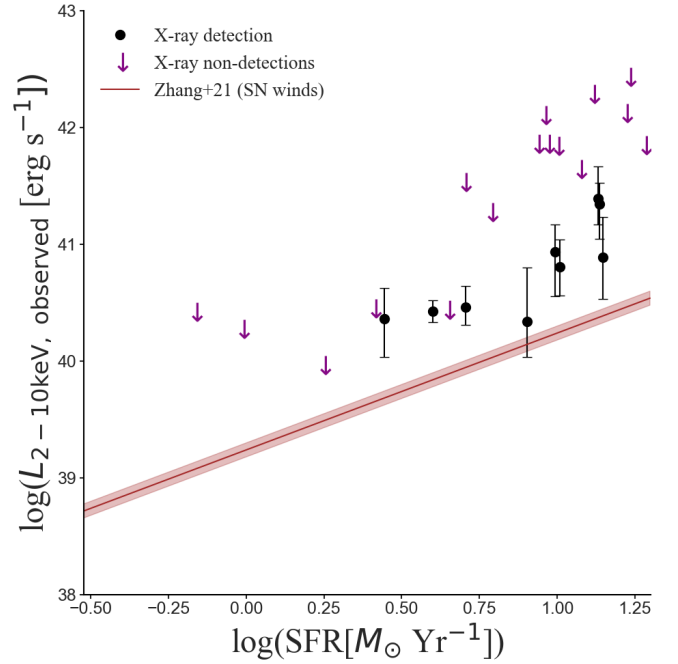


**Figure 5.** Similar to Fig. 1 but showing the X-ray emissions due to fast-radiative shocks from supernovae-driven winds as per Zhang (2021). The 2-10 keV X-ray luminosity of only one source falls within the range described by this calibration.

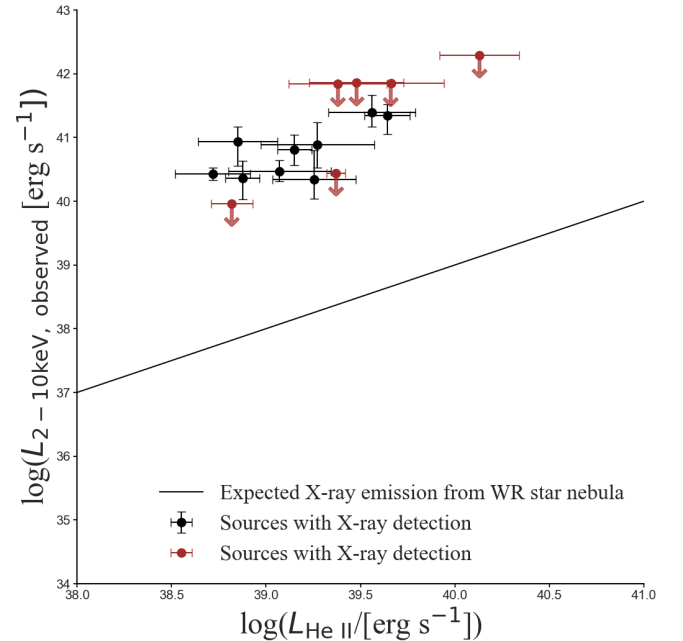


**Figure 6.** A plot showing He II $\lambda$ 4686 vs. X-ray luminosity for the 15 sources where  $S/N(\text{He II}\lambda 4686) > 3$ . The black dotted line describes the expected X-ray emission from WR stars if the observed He II $\lambda$ 4686 was fully produced by them.



In this section we combine the X-ray and He II $\lambda$ 4686 emissions and attempt to characterize the astrophysical origin of the X-ray emission and to identify any potential signature of massive BHs.

#### 4.1. Stellar origin?

##### 4.1.1. Fast radiative shocks:

A popular hypothesis behind the He II $\lambda$ 4686 and X-ray emission in starburst galaxies is the fast radiative shocks due to supernovae-driven winds, which manifest as broad emission line components in the Balmer lines (Heckman et al. 1981; Izotov et al. 2011a; Zhang 2021) including H $\alpha$  (Wood et al. 2015). However, the  $L_{2-10 \text{ keV}}$  produced by these shocks are about an order of magnitude lower than that seen in our sources as seen in Fig. 5. The only exception is J002101.0+005248 where the observed  $L_{2-10 \text{ keV}}$  is described by the X-ray luminosity vs. SFR calibrations for these shocks (Zhang 2021). Therefore, for the majority of our sources fast radiative shocks cannot solely describe the observed X-ray emission.

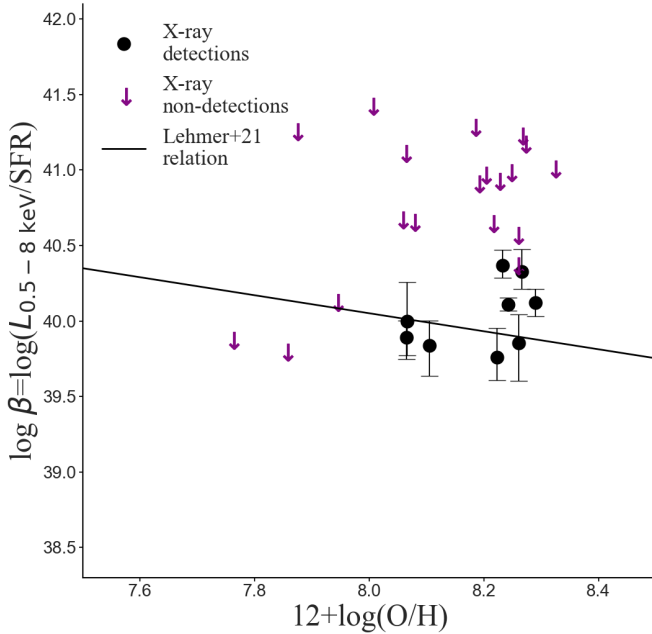


**Figure 7.** A plot showing  $\beta$  and metallicity relation for sources with X-ray detections (in black circles) and non-detections (in purple arrows). If the X-ray emission is dominated by HMXBs, we would expect an anti-correlation between SFR and  $12 + \log(\text{O}/\text{H})$ , as shown by the yellow line denoting the calibration by Lehmer et al. (2022). However, no such anti-correlation is observed.

##### 4.1.2. Wolf-Rayet stars:

If we assume that both the X-ray and He II $\lambda$ 4686 are produced by a Wolf-Rayet (WR) star nebula, the diversity in

He II $\lambda$ 4686 line profiles challenges this notion. WR stars are often characterized by their broad He II $\lambda$ 4686 profile ( $\sigma_{\text{He II}} > 300 \text{ km s}^{-1}$ ) (Crowther 2000, 2007). However, there are six sources where the He II $\lambda$ 4686 velocity dispersion  $< 200 \text{ km s}^{-1}$ , in contrast to a broad He II $\lambda$ 4686 emission profile, that one would expect from WR stars.

The typical He II luminosity of a WR star is  $L_{\text{He II}} \sim 10^{36} \text{ erg s}^{-1}$  (Crowther 2007; Crowther et al. 2023). The observed He II $\lambda$ 4686 luminosity in our sample ranges between  $7 \times 10^{38} - 3 \times 10^{40} \text{ erg s}^{-1}$ . Assuming the entire He II $\lambda$ 4686 nebula being produced solely by WR stars, that would give us  $700 - 10^4$  WR stars in the galaxies. The typical 2-10 keV X-ray luminosity from WR stars is  $10^{34} \text{ erg s}^{-1}$  (White & Long 1986; Raassen et al. 2003). Therefore, the expected 2-10 keV X-ray luminosity from the WR star nebula would be  $7 \times 10^{36} - 10^{38} \text{ erg s}^{-1}$ , which is about two orders of magnitude lower than the observed  $L_{2-10 \text{ keV}}$  (see Fig. 6). Therefore, WR stars cannot produce the observed X-ray and He II $\lambda$ 4686 emission.

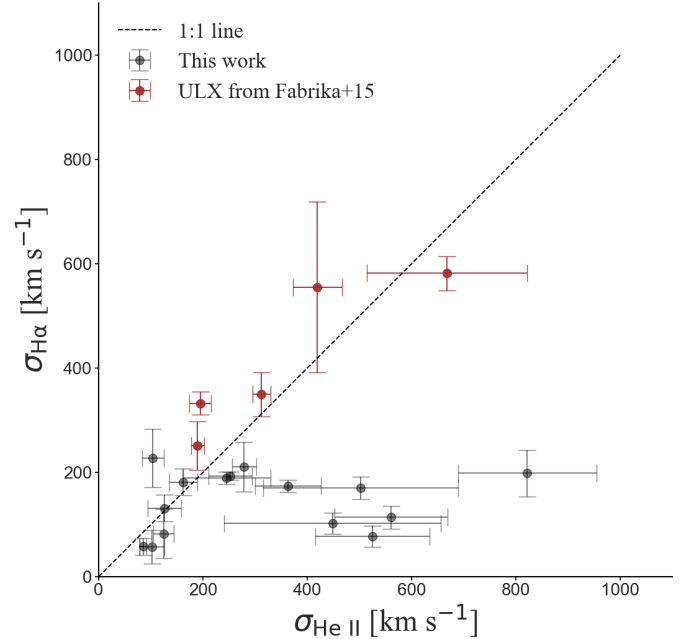


**Figure 8.** A scatter plot showing the velocity dispersion of the H $\alpha$  broad component ( $\sigma_{\text{H}\alpha, \text{ broad}}$ ) against that of He II $\lambda$ 4686 ( $\sigma_{\text{He II}\lambda 4686}$ ). The ULX from Fabrika et al. (2015) are shown in red. The black dashed line represents where  $\sigma_{\text{H}\alpha, \text{ broad}} = \sigma_{\text{He II}\lambda 4686}$ . In most our sources  $\sigma_{\text{He II}\lambda 4686}$  is systematically much higher than  $\sigma_{\text{H}\alpha, \text{ broad}}$ , as opposed to the ULXs.

#### 4.2. HMXB/ULX?

We compare the normalized 0.5-8 keV X-ray luminosity,  $\beta = L_{0.5-8 \text{ keV}}/\text{SFR}$ , against  $12 + \log(\text{O}/\text{H})$  for both X-ray detected and non-detected sources, as illustrated in Fig. 7.

We convert the 0.5-7 keV broadband X-ray luminosity to 0.5-8 keV X-ray luminosity using a conversion factor of 1.12. We observe that among the 9 X-ray detected sources, the normalized X-ray luminosity ( $\beta$ ) in 5 of them is consistent with an anticorrelation with  $12 + \log(\text{O}/\text{H})$  (Lehmer et al. 2021). This correlation is primarily due to the large uncertainties in X-ray luminosities. Lehmer et al. (2021) suggested that in low-metallicity ( $12 + \log(\text{O}/\text{H}) = 4.9.2$ ) dwarf galaxies, the number of high-mass X-ray binaries increases with decreasing metallicity, resulting in elevated X-ray emission. The authors proposed that the majority of the X-ray emission originates from X-ray binaries with 2-10 keV X-ray luminosities exceeding  $10^{38} \text{ erg s}^{-1}$ , commonly known as ULXs. However, ULXs could either be (i) super-Eddington accretors or (ii) intermediate-mass black holes (IMBHs). However, in 4 other sources with  $> 3\sigma$  X-ray detection, there is an excess X-ray emission in comparison to the Lehmer et al. (2021) correlation. To comprehensively understand the origin of the X-ray emission, we need to determine which of these two scenarios is most consistent with our multi-wavelength observations.

#### 4.2.1. Super-Eddington accretor:

To produce the observed X-ray luminosity in the 2-10 keV range ( $L_{2-10 \text{ keV}} > 10^{40.5} \text{ erg s}^{-1}$ ), both a  $2 M_{\odot}$  neutron star (the heaviest neutron star) and a  $100 M_{\odot}$  black hole (the heaviest possible stellar mass black hole) necessitate a super-Eddington accretion rate for sources with X-ray detection. For X-ray non-detected sources, if the mentioned upper limit of  $L_{2-10 \text{ keV}}$  is their 2-10 keV X-ray luminosity, then a super-Eddington accretion is also required. In a super-Eddington accretion scenario, a strong outflow should be generated at the accretion disk surface via radiation pressure force (Shakura & Sunyaev 1973; Ohsuga et al. 2005). This wind manifests as broad He II  $\lambda 4686$  and  $\text{H}\alpha$  lines, with the Balmer lines expected to be broader than He II  $\lambda 4686$  since they originate from regions of the wind situated farther from the source and have already gained speed (Fabrika et al. 2015). However, a study by Fabrika et al. (2015) on known super-Eddington accretors reveals that the line width of broad He II  $\lambda 4686$  and  $\text{H}\alpha$  would be strongly correlated with  $R^2 = 0.9$ . Importantly, we find a very weak correlation between the broad  $\text{H}\alpha$  and He II  $\lambda 4686$  line profiles with  $R^2 = 0.15$  as seen in Fig. 8. Additionally, the velocity dispersion of broad  $\text{H}\alpha$  is systematically lower than that of He II  $\lambda 4686$  and the broad  $\text{H}\alpha$  traces the ionized gas shocked by supernova-driven winds. Therefore, it is evident that the compact X-ray emitting source is not a super-Eddington accretor. Consequently, a black hole with  $M_{\text{BH}} > 100 M_{\odot}$  is necessary to produce the observed X-ray and He II  $\lambda 4686$  emission. Together with X-ray, He II emission, their mis-

sion line ratios are consistent with a low-metallicity low-luminosity AGN origin.

#### 4.2.2. Intermediate mass black holes/low-luminosity AGN:

By adopting a bolometric correction factor,  $\kappa_{2-10 \text{ keV}} = 20$ , the bolometric luminosity,  $L_{\text{bol}} = \kappa_{2-10 \text{ keV}} L_{2-10 \text{ keV}} = (4 \times 10^{40} - 7 \times 10^{42}) \text{ erg s}^{-1}$ , can be easily produced by a sub-Eddington LLAGN harboring an intermediate mass black hole (IMBH) with  $M_{\text{BH}} < 10^5 M_{\odot}$ . Assuming the broad  $\text{H}\alpha$  component is due to the gravitational potential of massive BHs, the BH mass for these sources will range between  $9.8 \times 10^3 - 4.9 \times 10^5 M_{\odot}$  (Greene & Ho 2005).

*Implication on reionization:* Traditionally, IMBHs have been believed to have a BH mass upper limit of  $10^5 M_{\odot}$  (Reines et al. 2014; Barrows et al. 2019). Recent studies suggest that IMBHs could have BH masses up to  $10^6 M_{\odot}$  (Zuo et al. 2024). LLAGN can have ionizing photon production rates significantly higher than their host galaxies, each producing up to  $\log(\dot{N}/\text{s}^{-1}) \sim 51$  (Kubota & Done 2018; Yung et al. 2021), and could have contributed largely to the ionizing photon budget during the Epoch of Reionization. Particularly, recent JWST detection of many high-redshift ‘‘little red dots’’ has implied a higher than expected AGN fraction, as high as 71% (e.g. Kocevski et al. 2023, 2024; Larson et al. 2023, also see Habouzit 2024 for a comprehensive discussions of JWST-detected AGN in the context of state-of-the-art cosmological simulations), and has rekindled discussions on their role in cosmic IGM reionization. While these LLAGN could be quite efficient at producing ionizing photons, their overall contribution depends on their number density and ionizing photon escape fraction, which remains unknown. Future multi-wavelength observations including JWST, ALMA are key to our understanding on their contribution in the producing the LyC photons.

## 5. CONCLUSION

We have searched the archival Chandra data for a sample of 900 Green Peas, with observations available only for 29 sources. To grasp the origin of X-ray emission in these sources, we examined the presence of the high-ionization emission line He II  $\lambda 4686$  and analyzed the  $\text{H}\alpha$  emission line profile in these 29 sources. Additionally, we supplemented the optical and X-ray observations with mid-infrared WISE observations which available for 25 out of 29 sources. We report that:

- 9 out of 29 sources show X-ray detection over  $3\sigma$  confidence. The 2-10 keV X-ray luminosity for two sources exceed  $10^{41} \text{ erg s}^{-1}$ , making them strong candidates for IMBH.

- He II $\lambda$ 4686 is detected over  $3\sigma$  confidence in 15 out of 29 sources. 8 out of 9 sources with X-ray detection show He II $\lambda$ 4686 detection.
- He II $\lambda$ 4686 shows a diversity in line-width,  $\sigma_{\text{He II}\lambda 4686} = 85 - 821 \text{ km s}^{-1}$ . In 9 out of 15 sources  $\sigma_{\text{He II}\lambda 4686}$  exceed  $200 \text{ km s}^{-1}$  suggesting presence of turbulent gas.
- The H $\alpha$  emission line in all 15 sources with He II $\lambda$ 4686 detection, requires two-Gaussian components (including a broad Gaussian), suggesting possible presence of winds. The broad Gaussian component most likely traces the moderately turbulent gas,  $\sigma_{\text{H}\alpha, \text{ broad}} < 230 \text{ km s}^{-1}$ .
- The emission line ratios such as [O III]/H $\beta$  and [N II]/H $\alpha$  for these sources are consistent with the narrow-line region of low-metallicity AGN.
- The WISE color information is available for 25 sources, including 9 sources with X-ray detection and 16 sources with X-ray non-detection. 2 out of 9 X-ray detected sources are consistent with AGN signature (Jarrett et al. 2011). 10 out of 16 X-ray non-detected sources are consistent with MIR colors of AGN.
- The 2-10 keV X-ray luminosity produced by fast-radiative shocks from supernovae and Wolf-Rayet stars is at least an order of magnitude lower than the observed X-ray luminosity.
- The normalized 0.5-8 keV X-ray luminosity of 5 X-ray detected sources are consistent with HMXB signature. However, the X-ray luminosity could only be produced by either (i) a super-Eddington accretor, or (ii) an IMBH/LLAGN.
- The H $\alpha$  and He II $\lambda$ 4686 linewidths show a weak correlation, as opposed to that expected from super-Eddington accretors.
- The observed X-ray could be then described by an LLAGN ( $M_{\text{BH}} = 10^4 - 10^6 M_{\odot}$ ), showing that LLAGN indeed exist in these GPs.

## ACKNOWLEDGEMENT

The material is based upon work supported by NASA under award number 80GSFC21M0002.

Z.Y.Z. acknowledges the support by the National Science Foundation of China (12022303) and the China-Chile Joint Research Fund (CCJRF No. 1906). We also acknowledge the science research grants from the China Manned Space Project with NO. CMS-CSST-2021-A04, CMS-CSST-2021-A07. F.T.Y. acknowledges the support by the Funds for Key Programs of Shanghai Astronomical Observatory (No. E195121009) and the Natural Science Foundation of Shanghai (Project Number: 21ZR1474300).

Funding for the Sloan Digital Sky Survey V has been provided by the Alfred P. Sloan Foundation, the Heising-Simons Foundation, the National Science Foundation, and the Participating Institutions. SDSS acknowledges support and resources from the Center for High-Performance Computing at the University of Utah. The SDSS web site is [www.sdss.org](http://www.sdss.org).

SDSS is managed by the Astrophysical Research Consortium for the Participating Institutions of the SDSS Collaboration, including the Carnegie Institution for Science, Chilean National Time Allocation Committee (CNTAC) ratified researchers, the Gotham Participation Group, Harvard University, Heidelberg University, The Johns Hopkins University, L'École polytechnique fédérale de Lausanne (EPFL), Leibniz-Institut für Astrophysik Potsdam (AIP), Max-Planck-Institut für Astronomie (MPIA Heidelberg), Max-Planck-Institut für Extraterrestrische Physik (MPE), Nanjing University, National Astronomical Observatories of China (NAOC), New Mexico State University, The Ohio State University, Pennsylvania State University, Smithsonian Astrophysical Observatory, Space Telescope Science Institute (STScI), the Stellar Astrophysics Participation Group, Universidad Nacional Autónoma de México, University of Arizona, University of Colorado Boulder, University of Illinois at Urbana-Champaign, University of Toronto, University of Utah, University of Virginia, Yale University, and Yunnan University.

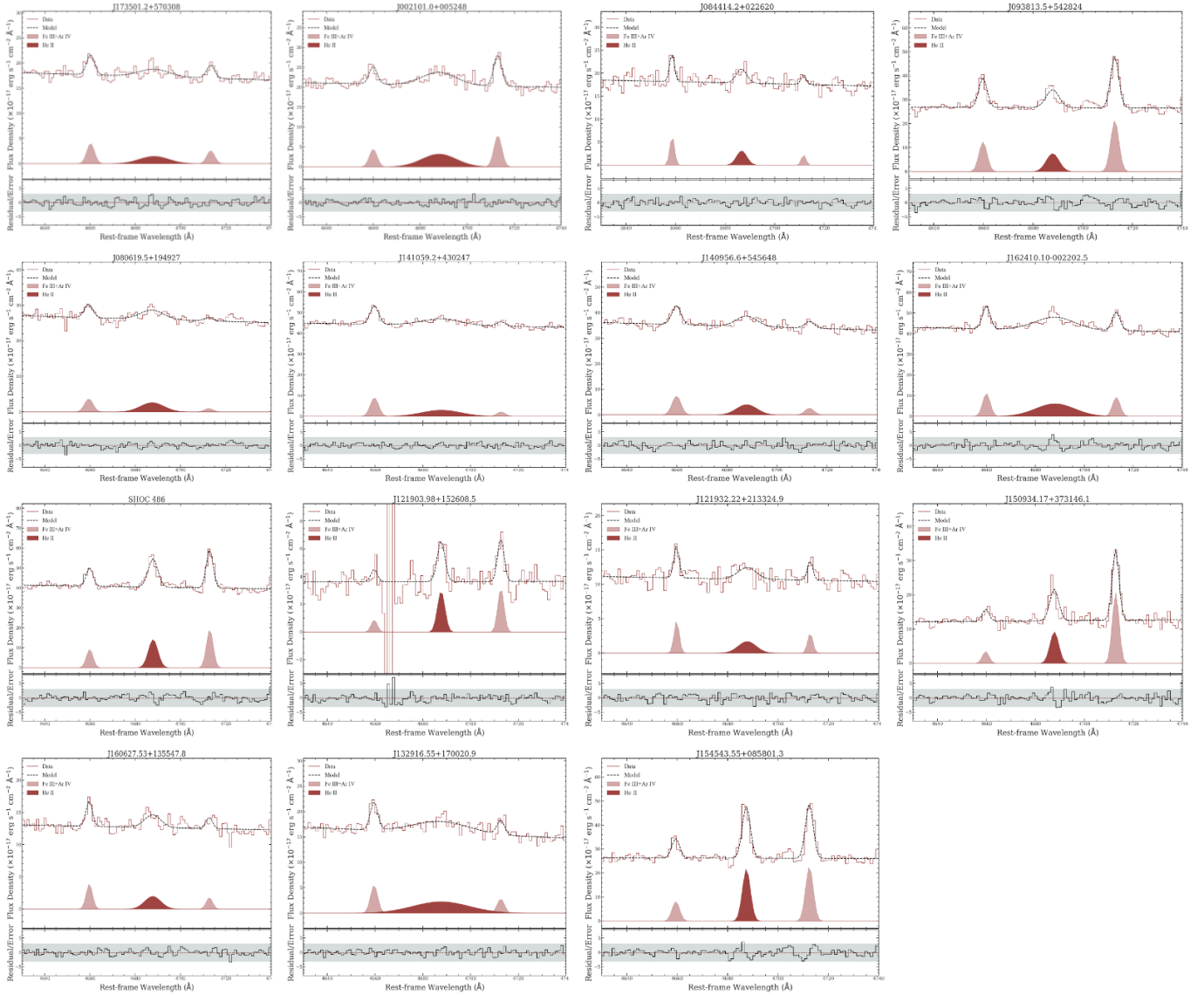
## REFERENCES

- Abel, N. P., & Satyapal, S. 2008, *ApJ*, 678, 686, doi: [10.1086/529013](https://doi.org/10.1086/529013)
- Alexander, D. M., & Hickox, R. C. 2012, *NewAR*, 56, 93, doi: [10.1016/j.newar.2011.11.003](https://doi.org/10.1016/j.newar.2011.11.003)
- Atek, H., Labbé, I., Furtak, L. J., et al. 2024, *Nature*, 626, 975, doi: [10.1038/s41586-024-07043-6](https://doi.org/10.1038/s41586-024-07043-6)
- Bachetti, M., Harrison, F. A., Walton, D. J., et al. 2014, *Nature*, 514, 202, doi: [10.1038/nature13791](https://doi.org/10.1038/nature13791)
- Baldwin, J. A., Phillips, M. M., & Terlevich, R. 1981, *PASP*, 93, 5, doi: [10.1086/130766](https://doi.org/10.1086/130766)
- Barrows, R. S., Mezcua, M., & Comerford, J. M. 2019, *ApJ*, 882, 181, doi: [10.3847/1538-4357/ab338a](https://doi.org/10.3847/1538-4357/ab338a)

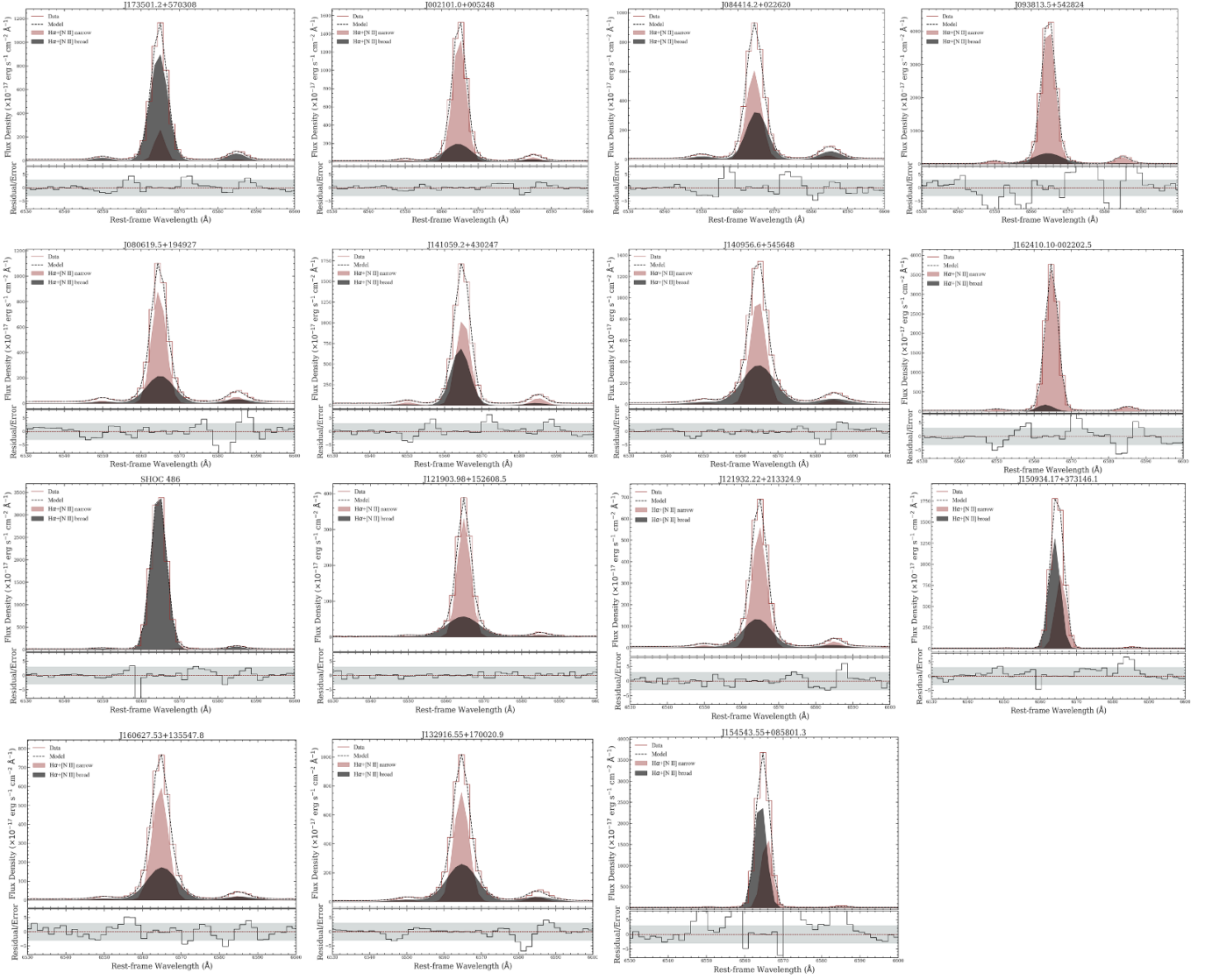
- Basu-Zych, A., & Scharf, C. 2004, *ApJL*, 615, L85, doi: [10.1086/426390](https://doi.org/10.1086/426390)
- Birchall, K. L., Watson, M. G., Aird, J., & Starling, R. L. C. 2022, *MNRAS*, 510, 4556, doi: [10.1093/mnras/stab3573](https://doi.org/10.1093/mnras/stab3573)
- Brorby, M., Kaaret, P., Prestwich, A., & Mirabel, I. F. 2016, *MNRAS*, 457, 4081, doi: [10.1093/mnras/stw284](https://doi.org/10.1093/mnras/stw284)
- Calhau, J., Sobral, D., Santos, S., et al. 2020, *MNRAS*, 493, 3341, doi: [10.1093/mnras/staa476](https://doi.org/10.1093/mnras/staa476)
- Cardamone, C., Schawinski, K., Sarzi, M., et al. 2009, *MNRAS*, 399, 1191, doi: [10.1111/j.1365-2966.2009.15383.x](https://doi.org/10.1111/j.1365-2966.2009.15383.x)
- Crowther, P. A. 2000, *A&A*, 356, 191, doi: [10.48550/arXiv.astro-ph/0001226](https://doi.org/10.48550/arXiv.astro-ph/0001226)
- . 2007, *ARA&A*, 45, 177, doi: [10.1146/annurev.astro.45.051806.110615](https://doi.org/10.1146/annurev.astro.45.051806.110615)
- Crowther, P. A., Rate, G., & Bestenlehner, J. M. 2023, *MNRAS*, 521, 585, doi: [10.1093/mnras/stad418](https://doi.org/10.1093/mnras/stad418)
- Diaz, Y., Arévalo, P., Hernández-García, L., et al. 2020, *MNRAS*, 496, 5399, doi: [10.1093/mnras/staa1762](https://doi.org/10.1093/mnras/staa1762)
- Fabrika, S., Ueda, Y., Vinokurov, A., Sholukhova, O., & Shidatsu, M. 2015, *Nature Physics*, 11, 551, doi: [10.1038/nphys3348](https://doi.org/10.1038/nphys3348)
- Fruscione, A., McDowell, J. C., Allen, G. E., et al. 2006, in *Society of Photo-Optical Instrumentation Engineers (SPIE) Conference Series*, Vol. 6270, *Observatory Operations: Strategies, Processes, and Systems*, ed. D. R. Silva & R. E. Doxsey, 62701V, doi: [10.1117/12.671760](https://doi.org/10.1117/12.671760)
- Giallongo, E., Grazian, A., Fiore, F., et al. 2015, *A&A*, 578, A83, doi: [10.1051/0004-6361/201425334](https://doi.org/10.1051/0004-6361/201425334)
- Gilfanov, M., & Merloni, A. 2014, *SSRv*, 183, 121, doi: [10.1007/s11214-014-0071-5](https://doi.org/10.1007/s11214-014-0071-5)
- Greene, J. E., & Ho, L. C. 2005, *ApJ*, 627, 721, doi: [10.1086/430590](https://doi.org/10.1086/430590)
- Grimm, H. J., Gilfanov, M., & Sunyaev, R. 2003, *MNRAS*, 339, 793, doi: [10.1046/j.1365-8711.2003.06224.x](https://doi.org/10.1046/j.1365-8711.2003.06224.x)
- Groves, B. A., Heckman, T. M., & Kauffmann, G. 2006, *Monthly Notices of the Royal Astronomical Society*, doi: [10.1111/j.1365-2966.2006.10812.x](https://doi.org/10.1111/j.1365-2966.2006.10812.x)
- Habouzit, M. 2024, *arXiv e-prints*, arXiv:2405.05319, doi: [10.48550/arXiv.2405.05319](https://doi.org/10.48550/arXiv.2405.05319)
- Haines, C. P., Pereira, M. J., Sanderson, A. J. R., et al. 2012, *ApJ*, 754, 97, doi: [10.1088/0004-637X/754/2/97](https://doi.org/10.1088/0004-637X/754/2/97)
- Harikane, Y., Zhang, Y., Nakajima, K., et al. 2023, *arXiv e-prints*, arXiv:2303.11946, doi: [10.48550/arXiv.2303.11946](https://doi.org/10.48550/arXiv.2303.11946)
- Harish, S., Malhotra, S., Rhoads, J. E., et al. 2021, *arXiv e-prints*, arXiv:2105.13400, doi: [10.48550/arXiv.2105.13400](https://doi.org/10.48550/arXiv.2105.13400)
- Heckman, T. M., Miley, G. K., van Breugel, W. J. M., & Butcher, H. R. 1981, *ApJ*, 247, 403, doi: [10.1086/159050](https://doi.org/10.1086/159050)
- Henry, A., Scarlata, C., Martin, C. L., & Erb, D. 2015, *ApJ*, 809, 19, doi: [10.1088/0004-637X/809/1/19](https://doi.org/10.1088/0004-637X/809/1/19)
- Israel, G. L., Belfiore, A., Stella, L., et al. 2017, *Science*, 355, 817, doi: [10.1126/science.aai8635](https://doi.org/10.1126/science.aai8635)
- Izotov, Y. I., Guseva, N. G., Fricke, K. J., & Henkel, C. 2011a, *A&A*, 536, L7, doi: [10.1051/0004-6361/201118402](https://doi.org/10.1051/0004-6361/201118402)
- Izotov, Y. I., Guseva, N. G., & Thuan, T. X. 2011b, *ApJ*, 728, 161, doi: [10.1088/0004-637X/728/2/161](https://doi.org/10.1088/0004-637X/728/2/161)
- Jarrett, T. H., Cohen, M., Masci, F., et al. 2011, *ApJ*, 735, 112, doi: [10.1088/0004-637X/735/2/112](https://doi.org/10.1088/0004-637X/735/2/112)
- Jiang, T., Malhotra, S., Yang, H., & Rhoads, J. E. 2019, *ApJ*, 872, 146, doi: [10.3847/1538-4357/aaee79](https://doi.org/10.3847/1538-4357/aaee79)
- Juodžbalis, I., Conselice, C. J., Singh, M., et al. 2023, *MNRAS*, 525, 1353, doi: [10.1093/mnras/stad2396](https://doi.org/10.1093/mnras/stad2396)
- Kaaret, P., Feng, H., & Roberts, T. P. 2017, *ARA&A*, 55, 303, doi: [10.1146/annurev-astro-091916-055259](https://doi.org/10.1146/annurev-astro-091916-055259)
- Karino, S., & Miller, J. C. 2016, *MNRAS*, 462, 3476, doi: [10.1093/mnras/stw1180](https://doi.org/10.1093/mnras/stw1180)
- Kauffmann, G., Heckman, T. M., White, S. D. M., et al. 2003, *MNRAS*, 341, 33, doi: [10.1046/j.1365-8711.2003.06291.x](https://doi.org/10.1046/j.1365-8711.2003.06291.x)
- Kewley, L. J., Dopita, M. A., Sutherland, R. S., Heisler, C. A., & Trevena, J. 2001, *ApJ*, 556, 121, doi: [10.1086/321545](https://doi.org/10.1086/321545)
- Kim, K. J., Malhotra, S., Rhoads, J. E., & Yang, H. 2021, *ApJ*, 914, 2, doi: [10.3847/1538-4357/abf833](https://doi.org/10.3847/1538-4357/abf833)
- Kocevski, D. D., Onoue, M., Inayoshi, K., et al. 2023, *ApJL*, 954, L4, doi: [10.3847/2041-8213/ace5a0](https://doi.org/10.3847/2041-8213/ace5a0)
- Kocevski, D. D., Finkelstein, S. L., Barro, G., et al. 2024, *arXiv e-prints*, arXiv:2404.03576, doi: [10.48550/arXiv.2404.03576](https://doi.org/10.48550/arXiv.2404.03576)
- Kubota, A., & Done, C. 2018, *MNRAS*, 480, 1247, doi: [10.1093/mnras/sty1890](https://doi.org/10.1093/mnras/sty1890)
- Larson, R. L., Finkelstein, S. L., Kocevski, D. D., et al. 2023, *ApJL*, 953, L29, doi: [10.3847/2041-8213/ace619](https://doi.org/10.3847/2041-8213/ace619)
- Latimer, L. J., Reines, A. E., Bogdan, A., & Kraft, R. 2021, *ApJL*, 922, L40, doi: [10.3847/2041-8213/ac3af6](https://doi.org/10.3847/2041-8213/ac3af6)
- Lehmer, B. D., Alexander, D. M., Bauer, F. E., et al. 2010, *ApJ*, 724, 559, doi: [10.1088/0004-637X/724/1/559](https://doi.org/10.1088/0004-637X/724/1/559)
- Lehmer, B. D., Eufrazio, R. T., Basu-Zych, A., et al. 2022, *ApJ*, 930, 135, doi: [10.3847/1538-4357/ac63a7](https://doi.org/10.3847/1538-4357/ac63a7)
- Lehmer, B. D., Eufrazio, R. T., Tzanavaris, P., et al. 2019, *ApJS*, 243, 3, doi: [10.3847/1538-4365/ab22a8](https://doi.org/10.3847/1538-4365/ab22a8)
- Lehmer, B. D., Eufrazio, R. T., Basu-Zych, A., et al. 2021, *ApJ*, 907, 17, doi: [10.3847/1538-4357/abceec1](https://doi.org/10.3847/1538-4357/abceec1)
- Lin, D., Strader, J., Carrasco, E. R., et al. 2018, *Nature Astronomy*, 2, 656, doi: [10.1038/s41550-018-0493-1](https://doi.org/10.1038/s41550-018-0493-1)
- Madau, P., & Haardt, F. 2015, *ApJL*, 813, L8, doi: [10.1088/2041-8205/813/1/L8](https://doi.org/10.1088/2041-8205/813/1/L8)
- Malhotra, S., Rhoads, J. E., Finkelstein, S. L., et al. 2012, *ApJL*, 750, L36, doi: [10.1088/2041-8205/750/2/L36](https://doi.org/10.1088/2041-8205/750/2/L36)
- Malhotra, S., Wang, J. X., Rhoads, J. E., Heckman, T. M., & Norman, C. A. 2003, *ApJL*, 585, L25, doi: [10.1086/373917](https://doi.org/10.1086/373917)
- Marin, F., Churazov, E., Khabibullin, I., et al. 2023, *Nature*, 619, 41, doi: [10.1038/s41586-023-06064-x](https://doi.org/10.1038/s41586-023-06064-x)
- Mezcua, M., Civano, F., Marchesi, S., et al. 2018, *MNRAS*, 478, 2576, doi: [10.1093/mnras/sty1163](https://doi.org/10.1093/mnras/sty1163)

- Mineo, S., Gilfanov, M., Lehmer, B. D., Morrison, G. E., & Sunyaev, R. 2014, *MNRAS*, 437, 1698, doi: [10.1093/mnras/stt1999](https://doi.org/10.1093/mnras/stt1999)
- Mineo, S., Gilfanov, M., & Sunyaev, R. 2012, *MNRAS*, 426, 1870, doi: [10.1111/j.1365-2966.2012.21831.x](https://doi.org/10.1111/j.1365-2966.2012.21831.x)
- Naidu, R. P., Tacchella, S., Mason, C. A., et al. 2020, *ApJ*, 892, 109, doi: [10.3847/1538-4357/ab7cc9](https://doi.org/10.3847/1538-4357/ab7cc9)
- Nakajima, K., Ouchi, M., Isobe, Y., et al. 2023, arXiv e-prints, arXiv:2301.12825, doi: [10.48550/arXiv.2301.12825](https://doi.org/10.48550/arXiv.2301.12825)
- Nandra, K., Mushotzky, R. F., Arnaud, K., et al. 2002, *ApJ*, 576, 625, doi: [10.1086/341888](https://doi.org/10.1086/341888)
- Ohsuga, K., Mori, M., Nakamoto, T., & Mineshige, S. 2005, *ApJ*, 628, 368, doi: [10.1086/430728](https://doi.org/10.1086/430728)
- Pintore, F., Belfiore, A., Novara, G., et al. 2018, *MNRAS*, 477, L90, doi: [10.1093/mnras/sly048](https://doi.org/10.1093/mnras/sly048)
- Raassen, A. J. J., van der Hucht, K. A., Mewe, R., et al. 2003, *A&A*, 402, 653, doi: [10.1051/0004-6361:20030119](https://doi.org/10.1051/0004-6361:20030119)
- Ranalli, P., Comastri, A., & Setti, G. 2003, *A&A*, 399, 39, doi: [10.1051/0004-6361:20021600](https://doi.org/10.1051/0004-6361:20021600)
- Reines, A. E., Plotkin, R. M., Russell, T. D., et al. 2014, *ApJL*, 787, L30, doi: [10.1088/2041-8205/787/2/L30](https://doi.org/10.1088/2041-8205/787/2/L30)
- Rephaeli, Y., Gruber, D., & Persic, M. 1995, *A&A*, 300, 91
- Rhoads, J. E., Wold, I. G. B., Harish, S., et al. 2023, *ApJL*, 942, L14, doi: [10.3847/2041-8213/acaaf](https://doi.org/10.3847/2041-8213/acaaf)
- Ricci, C., Kara, E., Loewenstein, M., et al. 2020, *ApJL*, 898, L1, doi: [10.3847/2041-8213/ab91a1](https://doi.org/10.3847/2041-8213/ab91a1)
- Robertson, B. E., Ellis, R. S., Furlanetto, S. R., & Dunlop, J. S. 2015, *ApJL*, 802, L19, doi: [10.1088/2041-8205/802/2/L19](https://doi.org/10.1088/2041-8205/802/2/L19)
- Sabha, N., Witzel, G., Eckart, A., et al. 2010, *A&A*, 512, A2, doi: [10.1051/0004-6361/200913186](https://doi.org/10.1051/0004-6361/200913186)
- Satyapal, S., Abel, N. P., & Secrest, N. J. 2018, *ApJ*, 858, 38, doi: [10.3847/1538-4357/aab7f8](https://doi.org/10.3847/1538-4357/aab7f8)
- Satyapal, S., Kamal, L., Cann, J. M., Secrest, N. J., & Abel, N. P. 2021, *ApJ*, 906, 35, doi: [10.3847/1538-4357/abfbaf](https://doi.org/10.3847/1538-4357/abfbaf)
- Shakura, N. I., & Sunyaev, R. A. 1973, *A&A*, 24, 337
- She, R., Ho, L. C., Feng, H., & Cui, C. 2018, *ApJ*, 859, 152, doi: [10.3847/1538-4357/aabfe7](https://doi.org/10.3847/1538-4357/aabfe7)
- Singha, M., O’Dea, C. P., Gordon, Y. A., Lawlor-Forsyth, C., & Baum, S. A. 2021, *ApJ*, 918, 65, doi: [10.3847/1538-4357/ac06c7](https://doi.org/10.3847/1538-4357/ac06c7)
- Singha, M., Husemann, B., Urrutia, T., et al. 2022, *A&A*, 659, A123, doi: [10.1051/0004-6361/202040122](https://doi.org/10.1051/0004-6361/202040122)
- Singha, M., Winkel, N., Vaddi, S., et al. 2023, *ApJ*, 959, 107, doi: [10.3847/1538-4357/ad004d](https://doi.org/10.3847/1538-4357/ad004d)
- Sutton, A. D., Roberts, T. P., Gladstone, J. C., et al. 2013, *MNRAS*, 434, 1702, doi: [10.1093/mnras/stt1133](https://doi.org/10.1093/mnras/stt1133)
- Svoboda, J., Douna, V., Orlitová, I., & Ehle, M. 2019, *ApJ*, 880, 144, doi: [10.3847/1538-4357/ab2b39](https://doi.org/10.3847/1538-4357/ab2b39)
- Swartz, D. A., Soria, R., Tennant, A. F., & Yukita, M. 2011, *ApJ*, 741, 49, doi: [10.1088/0004-637X/741/1/49](https://doi.org/10.1088/0004-637X/741/1/49)
- Volonteri, M., Dubois, Y., Pichon, C., & Devriendt, J. 2016, *MNRAS*, 460, 2979, doi: [10.1093/mnras/stw1123](https://doi.org/10.1093/mnras/stw1123)
- Wang, J. X., Malhotra, S., Rhoads, J. E., & Norman, C. A. 2004, *ApJL*, 612, L109, doi: [10.1086/424799](https://doi.org/10.1086/424799)
- White, R. L., & Long, K. S. 1986, *ApJ*, 310, 832, doi: [10.1086/164736](https://doi.org/10.1086/164736)
- Winkel, N., Husemann, B., Singha, M., et al. 2023, *A&A*, 670, A3, doi: [10.1051/0004-6361/202244630](https://doi.org/10.1051/0004-6361/202244630)
- Wood, C. M., Tremonti, C. A., Calzetti, D., et al. 2015, *MNRAS*, 452, 2712, doi: [10.1093/mnras/stv1471](https://doi.org/10.1093/mnras/stv1471)
- Wright, E. L., Eisenhardt, P. R. M., Mainzer, A. K., et al. 2010, *AJ*, 140, 1868, doi: [10.1088/0004-6256/140/6/1868](https://doi.org/10.1088/0004-6256/140/6/1868)
- Xu, Y., Ouchi, M., Nakajima, K., et al. 2023, arXiv e-prints, arXiv:2310.06614, doi: [10.48550/arXiv.2310.06614](https://doi.org/10.48550/arXiv.2310.06614)
- Yang, G., Caputi, K. I., Papovich, C., et al. 2023, *ApJL*, 950, L5, doi: [10.3847/2041-8213/acd639](https://doi.org/10.3847/2041-8213/acd639)
- Yang, H., Malhotra, S., Gronke, M., et al. 2016, *ApJ*, 820, 130, doi: [10.3847/0004-637X/820/2/130](https://doi.org/10.3847/0004-637X/820/2/130)
- Yang, Y., Zabludoff, A., Tremonti, C., Eisenstein, D., & Davé, R. 2009, *ApJ*, 693, 1579, doi: [10.1088/0004-637X/693/2/1579](https://doi.org/10.1088/0004-637X/693/2/1579)
- Yung, L. Y. A., Somerville, R. S., Finkelstein, S. L., et al. 2021, *MNRAS*, 508, 2706, doi: [10.1093/mnras/stab2761](https://doi.org/10.1093/mnras/stab2761)
- . 2020a, *MNRAS*, 496, 4574, doi: [10.1093/mnras/staa1800](https://doi.org/10.1093/mnras/staa1800)
- Yung, L. Y. A., Somerville, R. S., Popping, G., & Finkelstein, S. L. 2020b, *MNRAS*, 494, 1002, doi: [10.1093/mnras/staa714](https://doi.org/10.1093/mnras/staa714)
- Zhang, X.-G. 2021, *MNRAS*, 502, 2508, doi: [10.1093/mnras/stab185](https://doi.org/10.1093/mnras/stab185)
- Zheng, Z.-Y., Malhotra, S., Wang, J.-X., et al. 2012, *ApJ*, 746, 28, doi: [10.1088/0004-637X/746/1/28](https://doi.org/10.1088/0004-637X/746/1/28)
- Zuo, W., Guo, H., Sun, J., et al. 2024, arXiv e-prints, arXiv:2405.11750, doi: [10.48550/arXiv.2405.11750](https://doi.org/10.48550/arXiv.2405.11750)

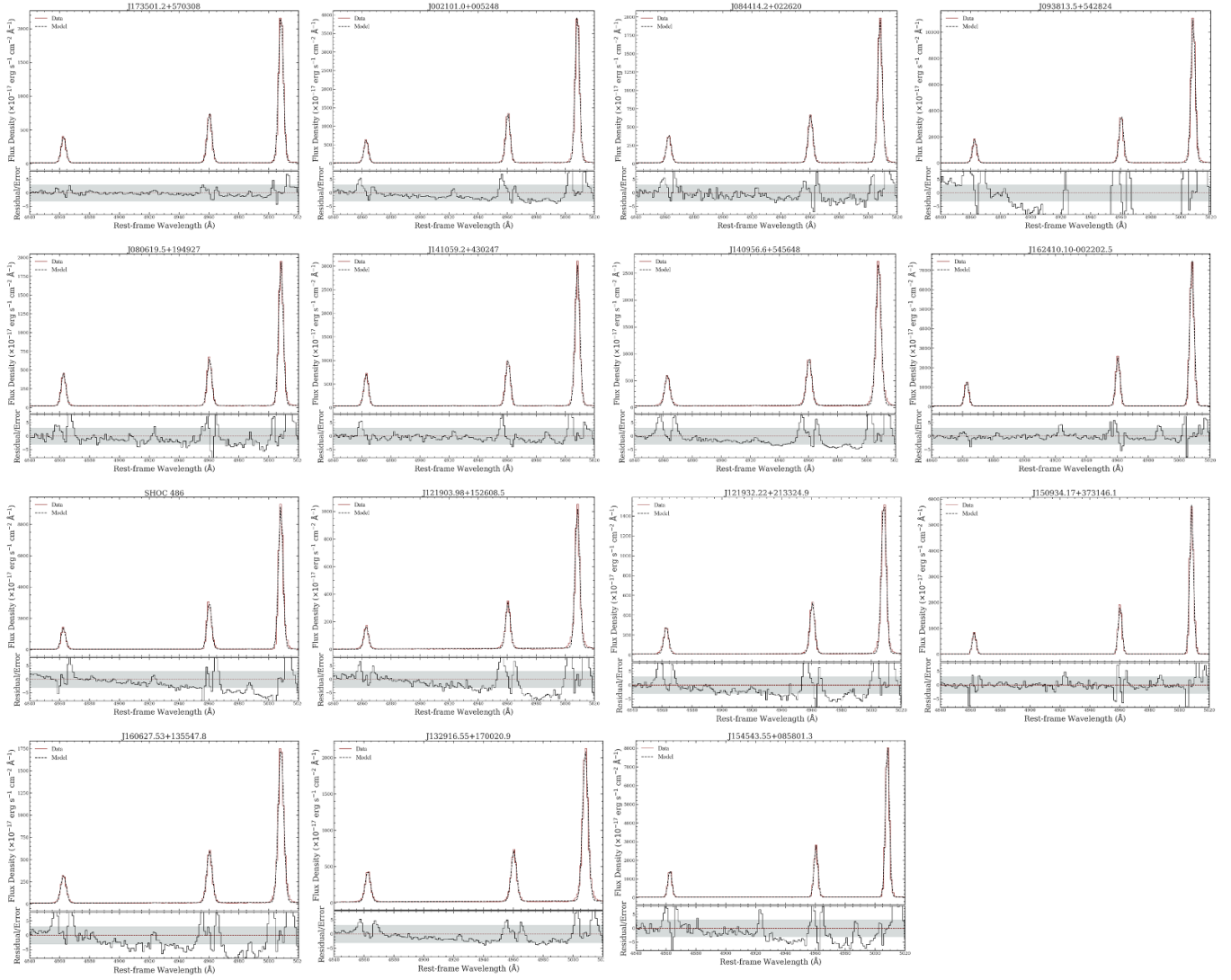
## 6. APPENDIX

6.1. *He II*λ4686 spectra

**Figure 9.** Top panel shows the source spectra centered on *He II*λ4686. The solid red line is the data and the black dashed line is the composite model of the 3 emission lines which are present: *Fe III*λ4658, *He II*λ4686, and *Ar IV*λ4711. The shaded regions show the individual models for the corresponding lines. The pink shaded region shows models for the *Fe III*λ4658 and *Ar IV*λ4711 lines. The red shaded regions shows the model for the *He II*λ4686 line. Additional details regarding the models/fit can be found in Section 3.2.1. The bottom panel shows residuals normalized by the error.

6.2.  $H\alpha+[N II]$  spectra

**Figure 10.** Top panel shows the source spectra centered on the  $H\alpha+[N II]\lambda\lambda 6548, 6584$  lines. The solid red line is the data and the black dashed line is the composite model of the emission lines. A multi-Gaussian model with both broad and narrow Gaussians was fit to the  $H\alpha$  and  $[N II]$  lines. The shaded regions show the components of the multi-Gaussian model. The pink shaded region shows the narrow Gaussian model, while the dark grey shaded region shows the broad Gaussian model. Additional details regarding the models/fit can be found in Section 3.2.2. The bottom panel shows residuals normalized by the error.

6.3.  $H\beta+[O III]$  spectra

**Figure 11.** Top panel shows the source spectra centered on the  $H\beta+[O III]\lambda\lambda 4959, 5007$  lines. The solid red line is the data and the black dashed line is the composite model of the emission lines. A single Gaussian model for each of the aforementioned emission lines was fit to the emission line complex. The bottom panel shows residuals normalized by the error. Adding additional Gaussian did not significantly improve the fit.